SCIENTIFIC REPORTS

OPEN

SUBJECT AREAS:
CHARACTERIZATION AND ANALYTICAL TECHNIQUES
TWO-DIMENSIONAL MATERIALS
SYNTHESIS AND PROCESSING
OPTICAL MATERIALS AND STRUCTURES

Received
21 August 2014

Accepted
19 January 2015

Published
13 February 2015

Correspondence and requests for materials should be addressed to L.D. (lundai@pku.edu.cn)

Measuring the Refractive Index of Highly Crystalline Monolayer MoS_2 with High Confidence

Hui Zhang[1,2], Yaoguang Ma[1], Yi Wan[1], Xin Rong[1], Ziang Xie[1], Wei Wang[1] & Lun Dai[1,2]

[1]State Key Lab for Mesoscopic Physics and School of Physics, Peking University, Beijing 100871, China, [2]Collaborative Innovation Center of Quantum Matter, Beijing 100871, China.

Monolayer molybdenum disulphide (MoS_2) has attracted much attention, due to its attractive properties, such as two-dimensional properties, direct bandgap, valley-selective circular dichroism, and valley Hall effect. However, some of its fundamental physical parameters, *e.g.* refractive index, have not been studied in detail because of measurement difficulties. In this work, we have synthesized highly crystalline monolayer MoS_2 on SiO_2/Si substrates via chemical vapor deposition (CVD) method and devised a method to measure their optical contrast spectra. Using these contrast spectra, we extracted the complex refractive index spectrum of monolayer MoS_2 in the wavelength range of 400 nm to 750 nm. We have analyzed the pronounced difference between the obtained complex refractive index spectrum and that of bulk MoS_2. The method presented here is effective for two-dimensional materials of small size. Furthermore, we have calculated the color contour plots of the contrast as a function of both SiO_2 thickness and incident light wavelength for monolayer MoS_2 using the obtained refractive index spectrum. These plots are useful for both fundamental study and device application.

In recent years, the discovery of various kinds of two-dimensional (2D) materials[1–4] has promoted low-dimensional physics research. Among these materials, monolayer MoS_2, a stable atomically thin structure with honeycomb lattice, has attracted much attention, because of its remarkable physical properties and novel applications, such as direct bandgap[2], strong spin-orbit coupling[5,6], valley-selective circular dichroism[7–10], valley Hall effect[11,12], nonlinear optical effect[13], and two-dimensional heterostructures[14–17]. Recent progress in the synthesis of highly crystalline monolayer MoS_2 with chemical vapor deposition (CVD) method[18–20] has made it a promising candidate for novel electronic and optoelectronic devices. Its complex refractive index in visible range is important, because many of its novel properties are closely related to this wavelength range. Beal *et al.* measured the complex refractive index of bulk MoS_2[21] in 1979. However, physical properties of a 2D material are usually very different from those of bulk material, especially for MoS_2, which has an indirect bandgap in bulk form and a direct bandgap in monolayer form[2]. Recently several groups have measured the optical constants of large-area CVD grown thin films of MoS_2 or other transition metal dichalcogenides using spectroscopic ellipsometry technique[22–24]. However, so far, it is still difficult to measure the refractive index of highly crystalline monolayer MoS_2 directly, because the highly crystalline monolayer MoS_2 flakes obtained by present methods (mechanical exfoliation, CVD *etc.*), are usually too small in size (~ tens of microns). In 2007, Blake *et al.* successfully visualized graphene under an optical microscope by utilizing the contrast of graphene on a SiO_2/Si substrate. Given the refractive index of graphene, the contrast can further be calculated based on the Fresnel law[25]. In our work, by improving the spatial resolution of a reflectance spectrum system via spatial filtering, we managed to obtain the optical contrast spectra of highly crystalline monolayer MoS_2. Then by curve fitting the relations between the contrast and SiO_2 thickness based on the Fresnel law, we obtained the complex refractive index spectrum of monolayer MoS_2 in the wavelength range of 400 nm to 750 nm, together with the confidence interval, which reflects the accuracy of the obtained refractive index. We have analyzed the pronounced difference between the obtained complex refractive index spectrum and that of bulk MoS_2. Furthermore, we have calculated the color contour plots of the contrast as a function of both SiO_2 thickness and incident light wavelength for monolayer MoS_2 using the obtained refractive index spectrum. These plots are useful for both fundamental study and device application.

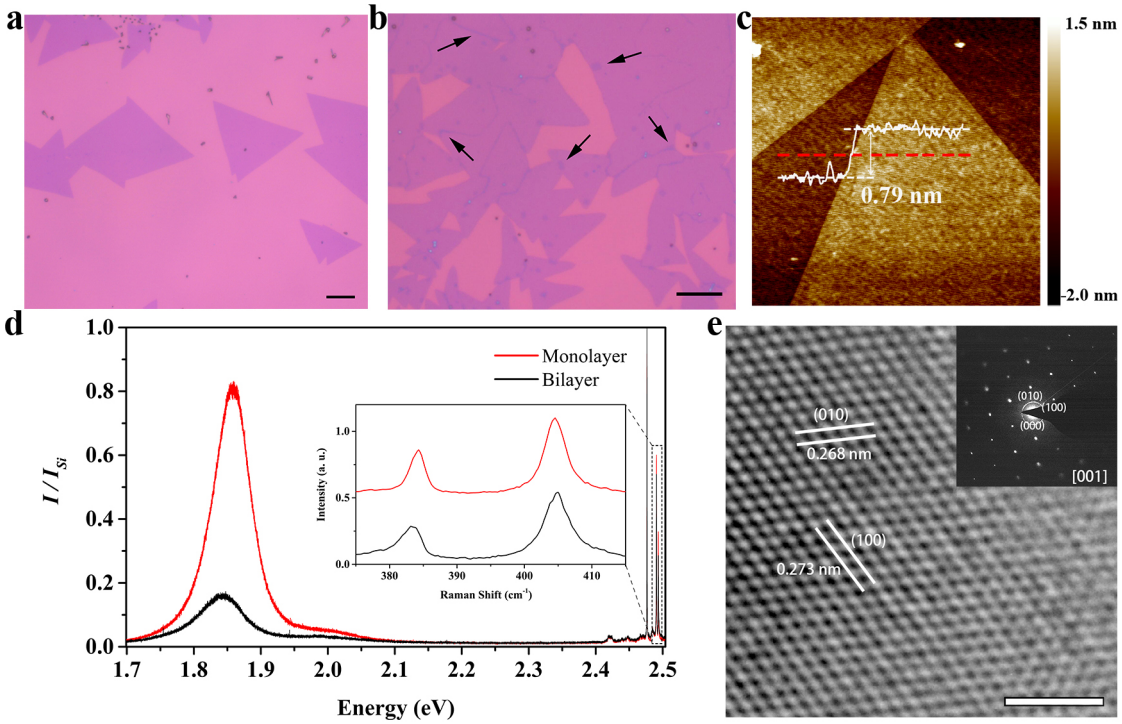

Figure 1 | Synthesis and characterization of monolayer MoS_2. (a) and (b) Optical images of typical MoS_2 on 280 nm SiO_2/Si substrates synthesized by CVD method. The growth durations are 10 min and 20 min, respectively. In (b), some monolayer MoS_2 islands overlapped with one another because of the longer growth time, as indicated with arrows. The scale bars correspond to 10 μm. (c) AFM image of two neighbored MoS_2 triangular islands. The white curve shows the thickness along the red dashed line. The scale bar corresponds to 0.5 μm. (d) Room-temperature PL spectra from monolayer MoS_2 (red) and bilayer MoS_2 (black). Peak height is normalized to the silicon Raman peak. Raman signals also appear in the PL spectra at the higher energy, details of which are shown in the inset. (e) HRTEM image of freely suspended monolayer MoS_2. The inset is the corresponding SAED pattern recorded along the [001] zone axis. The scale bar corresponds to 2 nm.

Results

Synthesis and characterization of highly crystalline monolayer MoS_2. In this work, we synthesized monolayer MoS_2 on various SiO_2/Si substrates by CVD method. Figures 1a, b show two typical optical images of the material grown on 280 nm SiO_2/Si substrates. The monolayer MoS_2 tend to form isolated triangular islands, with grain sizes ranging from a few microns to tens of microns. With increased growth time, some monolayer MoS_2 islands overlap with one another to form bilayer or multi-layer structures as indicated with the arrows in Fig. 1b. The thickness of a MoS_2 triangular island depicted in Fig. 1c, measured by an atomic force microscope (AFM), is about 0.79 nm, consistent with data from literatures[18,26].

The photoluminescence (PL) spectra of both monolayer and bilayer MoS_2 are shown in Figure 1d. Raman signals also appear in the PL spectra at higher energy, details of which are shown in the inset. For monolayer MoS_2, the PL spectrum is dominated by two peaks around 1.85 eV and 2.00 eV, which come from the A and B exciton transitions, respectively. The A and B excitons form at the K-point of the Brillouin zone, where strong spin-orbit coupling induces a splitting in the opposite spin valence bands by about 150 meV[2,10,27]. For bilayer MoS_2, the corresponding two exciton transition peaks are much weaker and exhibit a small red shift[27,28]. The Raman spectrum of monolayer MoS_2 consists of the E^1_{2g} (384.3 cm^{-1}) and A_{1g} (404.6 cm^{-1}) modes. Peak distance (Δ) of them is about 20.3 cm^{-1}. The E^1_{2g} and A_{1g} Raman modes of bilayer MoS_2 peak at 382.9 cm^{-1} and 404.8 cm^{-1} respectively, with a Δ of about 21.9 cm^{-1}. Peak distance between these two modes has been used to identify the number of layers of MoS_2[29]. For monolayer and bilayer MoS_2, the Δ values are about 18~20 cm^{-1} and 21~22 cm^{-1}, respectively[19,29]. Our results are consistent with these criteria.

We characterized crystal structure of the monolayer MoS_2 with a high-resolution transmission electron microscope (HRTEM), as shown in Fig. 1e. We can see clearly the {100} planes of MoS_2, with a lattice spacing of about 0.270 nm[18]. The HRTEM image, together with the corresponding selected area electron diffraction (SAED) shown in the inset, demonstrates that the monolayer MoS_2 is a single crystal with a hexagonal lattice structure.

Measuring the contrast spectra of monolayer MoS_2 on SiO_2/Si substrates. The schematic diagram of the experimental set-up for measuring the contrast spectrum of monolayer MoS_2 on a SiO_2/Si substrate is shown in Fig. 2a. An optical microscope equipped with a white light source was used to collect the reflected light signal from the sample. An optical fiber was used to selectively couple part of the reflected light signal into a spectrometer. In our case, the spatial resolution of the reflectance spectrum, which depends on both the objective lens magnification and the fiber diameter, is about 1 μm under 50× objective lens, smaller than the size of the monolayer MoS_2 islands. Figure 2b shows the reflectance spectra measured on monolayer MoS_2 grown on a 280 nm SiO_2/Si substrate and a bare 280 nm SiO_2/Si substrate respectively, for wavelengths ranging from 400 nm to 750 nm. Corresponding measured sites are labeled as A and B in the inset. The contrast of monolayer MoS_2 on a SiO_2/Si substrate can be defined as:

$$C = \frac{I_{substrate} - I_{MoS_2}}{I_{substrate} + I_{MoS_2}}, \quad (1)$$

where I_{MoS_2} and $I_{substrate}$ are the reflected light intensities from MoS_2 and the substrate, respectively. From the two reflectance spectra, we can calculate the contrast spectrum, which is also shown in Fig. 2b.

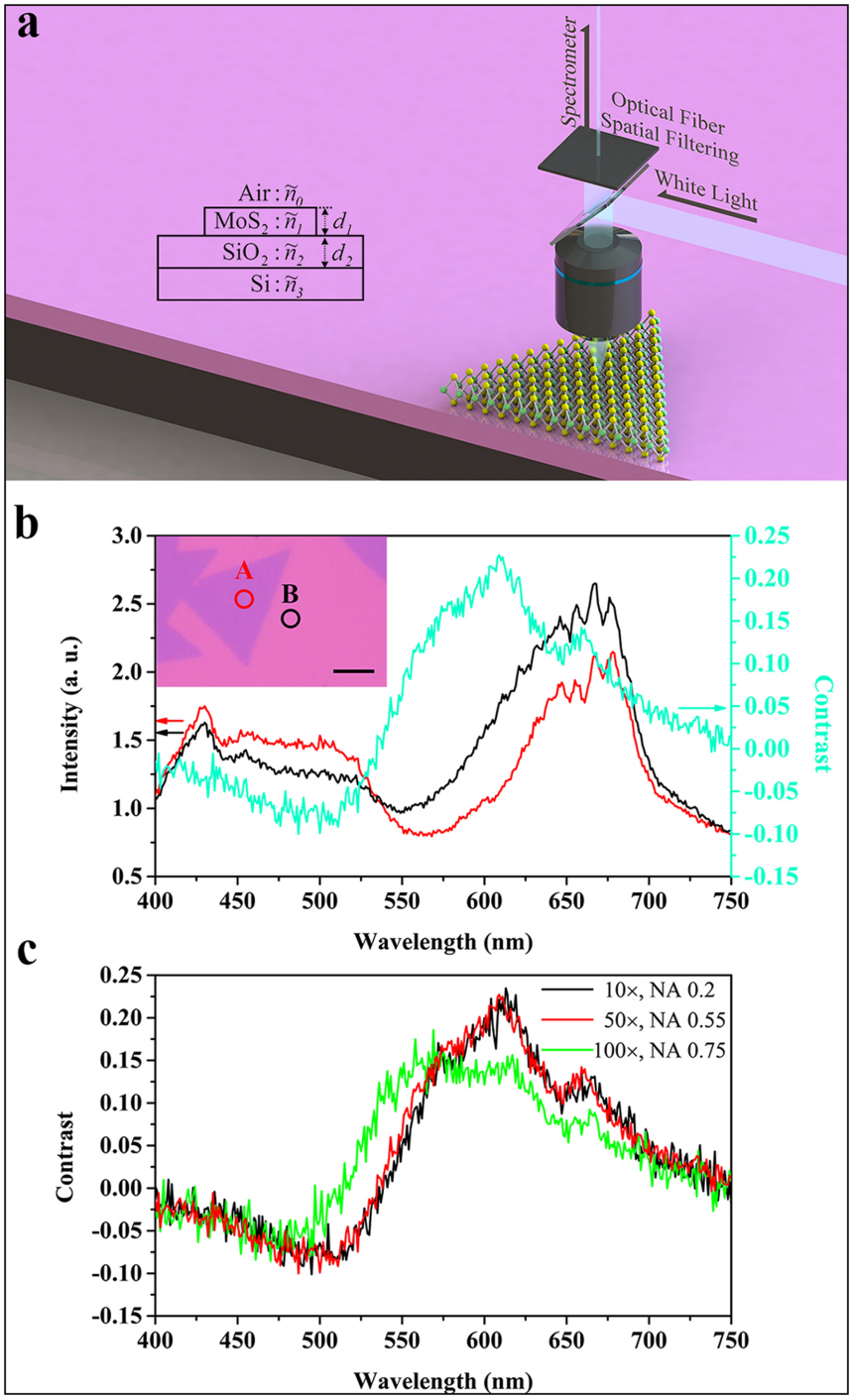

Figure 2 | Measurement of Spatially Resolved Contrast Spectrum. (a) The schematic diagram of the experimental set-up for measuring the contrast spectrum of monolayer MoS_2 on a SiO_2/Si substrate. Inset: The geometric structure of our sample. (b) The reflectance spectra measured on monolayer MoS_2 (red line) and 280 nm SiO_2/Si substrate (black line), respectively. Corresponding measured sites are labeled as A and B in the inset. The scale bar corresponds to 10 μm. The contrast spectrum extracted from the reflectance spectra is shown by the cyan line. (c) The contrast spectra of monolayer MoS_2 on a 281 nm SiO_2/Si substrate collected by using three objective lenses with different N. A. (0.2 (10×), 0.55 (50×), and 0.75 (100×)).

We assume normal incidence in the analysis of this work. We need to select a proper objective lens in order to minimize the error caused by the spatial Fourier components of the beam away from normal incidence[30]. On one hand, this requires the numerical aperture (N. A.) to be as small as possible. On the other hand, the lens with a smaller N. A. usually has smaller magnification, which in return reduces spatial resolution. Figures 2c shows three contrast spectra of monolayer MoS_2 on a 280 nm SiO_2/Si substrate, which were obtained by using objective lenses with N. A. of 0.2 (10×), 0.55 (50×), and 0.75 (100×), respectively. We can see that, apart from the spectrum collected by the lens with N. A. of 0.75, the contrast spectra collected by the other two lenses are similar, which means that the error caused by the beam away from normal incidence can be ignored when the N. A. is less than 0.55. Therefore, we used the 50× objective lens in our experiment to achieve optimal results.

Fitting the complex refractive index of monolayer MoS_2. For normal light incidence, the reflected light intensity from a sample

with the geometric structure shown in the inset of Fig. 2a can be written as[25]:

$$I=\left|\frac{r_1 e^{i(\Phi_1+\Phi_2)}+r_2 e^{-i(\Phi_1-\Phi_2)}+r_3 e^{-i(\Phi_1+\Phi_2)}+r_1 r_2 r_3 e^{i(\Phi_1-\Phi_2)}}{e^{i(\Phi_1+\Phi_2)}+r_1 r_2 e^{-i(\Phi_1-\Phi_2)}+r_1 r_3 e^{-i(\Phi_1+\Phi_2)}+r_2 r_3 e^{i(\Phi_1-\Phi_2)}}\right|^2, \quad (2)$$

where

$$r_1=\frac{\tilde{n}_0-\tilde{n}_1}{\tilde{n}_0+\tilde{n}_1},$$

$$r_2=\frac{\tilde{n}_1-\tilde{n}_2}{\tilde{n}_1+\tilde{n}_2},$$

$$r_3=\frac{\tilde{n}_2-\tilde{n}_3}{\tilde{n}_2+\tilde{n}_3},$$

are the relative indices of refraction. $\Phi_i=\frac{2\pi\tilde{n}_i d_i}{\lambda}$ is the phase shift due to the variation of the optical path, in which λ is the wavelength, d_i is thickness of related layer, and $\tilde{n}_i=n_i-ik_i$ is the complex refractive index of related material. The reflected light intensity from bare SiO_2/Si substrate can be obtained by setting $\tilde{n}_1=\tilde{n}_0\equiv 1$. Given the theoretical thickness for monolayer MoS_2 (d_1 = 0.63 nm[31]), the incident light wavelength, and the complex refractive indices of both SiO_2 and Si, we can obtain, from equations (1) and (2), the contrast of monolayer MoS_2 on a SiO_2/Si substrate as a function of both SiO_2 thickness (d_2) and complex refractive index of monolayer MoS_2 (n_1,k_1):

$$C=\frac{I_{substrate}-I_{MoS_2}}{I_{substrate}+I_{MoS_2}}=C(\tilde{n}_1,d_2)=C(n_1,k_1,d_2), \quad (3)$$

In order to obtain the complex refractive index spectrum of monolayer MoS_2, we measured contrast spectra of 26 monolayer MoS_2 samples on SiO_2/Si substrates with SiO_2 thickness ranging from ~130 nm to ~370 nm (Supplementary Fig. S1). From these contrast spectra, we extracted the relation between the contrast (C) and SiO_2 thickness (d_2) under a specific incident light wavelength, *e.g.* 651 nm, as shown in Fig. 3a (scattered open circles). The standard deviation of each point, indicated by its error bar, was obtained by multiple measurements. By curve fitting these data with equation (3) (the solid line), we obtained the complex refractive index of monolayer MoS_2 (n_1,k_1) at 651 nm. Similarly, we can obtain the C-d_2 relations under different incident light wavelength (from 400 nm to 750 nm). The resulting complex refractive index spectrum of monolayer MoS_2 is shown in Fig. 3b (scattered red circles), together with the confidence interval (red shadow), which corresponds to a 95% confidence level. The overall confidence interval is narrow, especially in the wavelength range from 550 nm to 700 nm, indicating that the result is with high confidence. We expect uniformity in sample properties, such as MoS_2 thickness, crystalline quality, and surface flatness, to contribute to the confidence interval. Therefore the narrow confidence interval in the wavelength range from 550 nm to 700 nm indicates good sample uniformity, which can be attributed to the stable double-temperature-zone CVD synthesis method employed in this work as well as the fundamental thickness uniformity of the layered 2D material (the thickness can only be one, two, or more mono-layers). The observed gradually broadened confidence interval at wavelengths below 450 nm and above 700 nm may result mainly from the poor signal-noise ratio of the measuring system in those wavelength ranges. The broadened confidence interval at the wavelength range of 450–525 nm may result from the poor signal-noise ratio of the measured optical contrast, which is related to the SiO_2 thickness employed. We can see in Fig. S1 that the absolute optical contrast of most of our samples are weaker in the wavelength range of 450–525 nm.

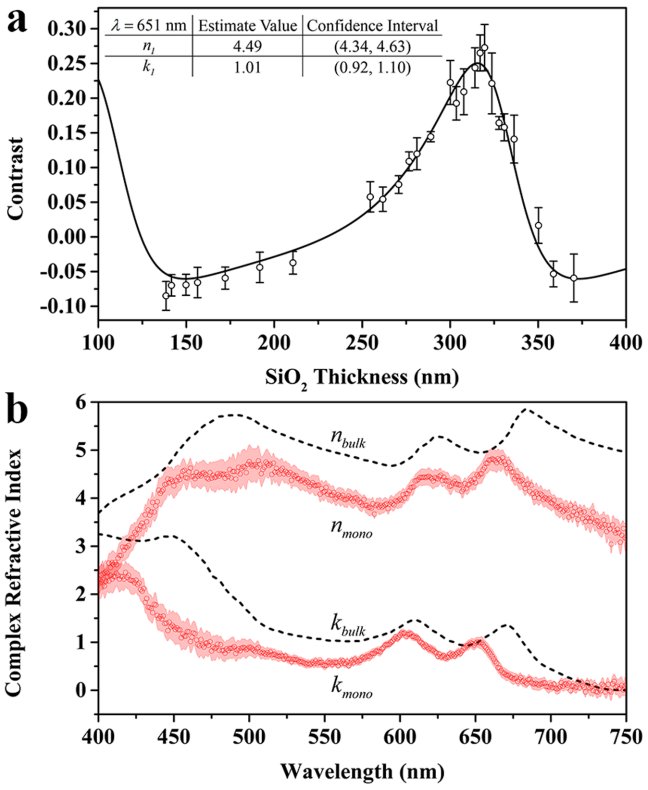

Figure 3 | Curve Fitting results of complex refractive index for monolayer MoS_2. (a) The contrast of monolayer MoS_2 as a function of the SiO_2 thickness under incident light wavelength of 651 nm (scattered open circles). The standard deviation of each point is shown by the error bar. The curve fitting result of the complex refractive index of monolayer MoS_2 at 651 nm is shown in the table in the inset. (b)The complex refractive index spectrum (scattered red circles) of monolayer MoS_2, obtained by curving fitting the relation between contrast and SiO_2 thickness relation with equation (3) under different incident light wavelength (from 400 nm to 750 nm). The red shadow shows the confidence interval, corresponding to a 95% confidence level. The black dashed lines show the complex refractive index spectrum of bulk MoS_2[21].

For comparison, we also plotted the complex refractive index spectrum of bulk MoS_2[21] in this figure with the black dashed lines. We can see that, for most wavelengths, the real and imaginary parts of the refractive index of monolayer MoS_2 are both lower than their bulk counterparts. In addition, for monolayer MoS_2, two peaks of the real part of the refractive index spectrum, located at 663 nm and 621 nm, exhibit a blue shift compared to their bulk counterparts (at 684 nm and 626 nm, respectively). Similarly, two peaks of the imaginary part (at 651 nm and 603 nm) also show a blue shift compared to their bulk counterparts (at 671 nm and 611 nm, respectively). Given that the imaginary part represents the electromagnetic wave absorption in a material, we attribute the two peaks of the imaginary part of the refractive index spectra to A and B exciton absorptions, respectively. The observed blue shifts of exciton absorption of monolayer MoS_2 compared to their bulk counterparts may be due to the difference of A and B excitons energy in bulk and monolayer MoS_2[2,27]. It is worth noting that, compared to the exciton emission peaks (located at 1.85 eV and 2.00 eV) shown in Fig. 1d, the observed A and B exciton absorption peaks of monolayer MoS_2 (located at 651 nm and 603 nm, *i.e.* 1.90 eV and 2.06 eV) also show a blue shift. This phenomenon results from the well-known Stokes shift between absorption and emission[32]. There also exists a peak near 400 nm for the imaginary part spectrum of monolayer MoS_2, which may be related to the convoluted C and D excitons[28,33]. The

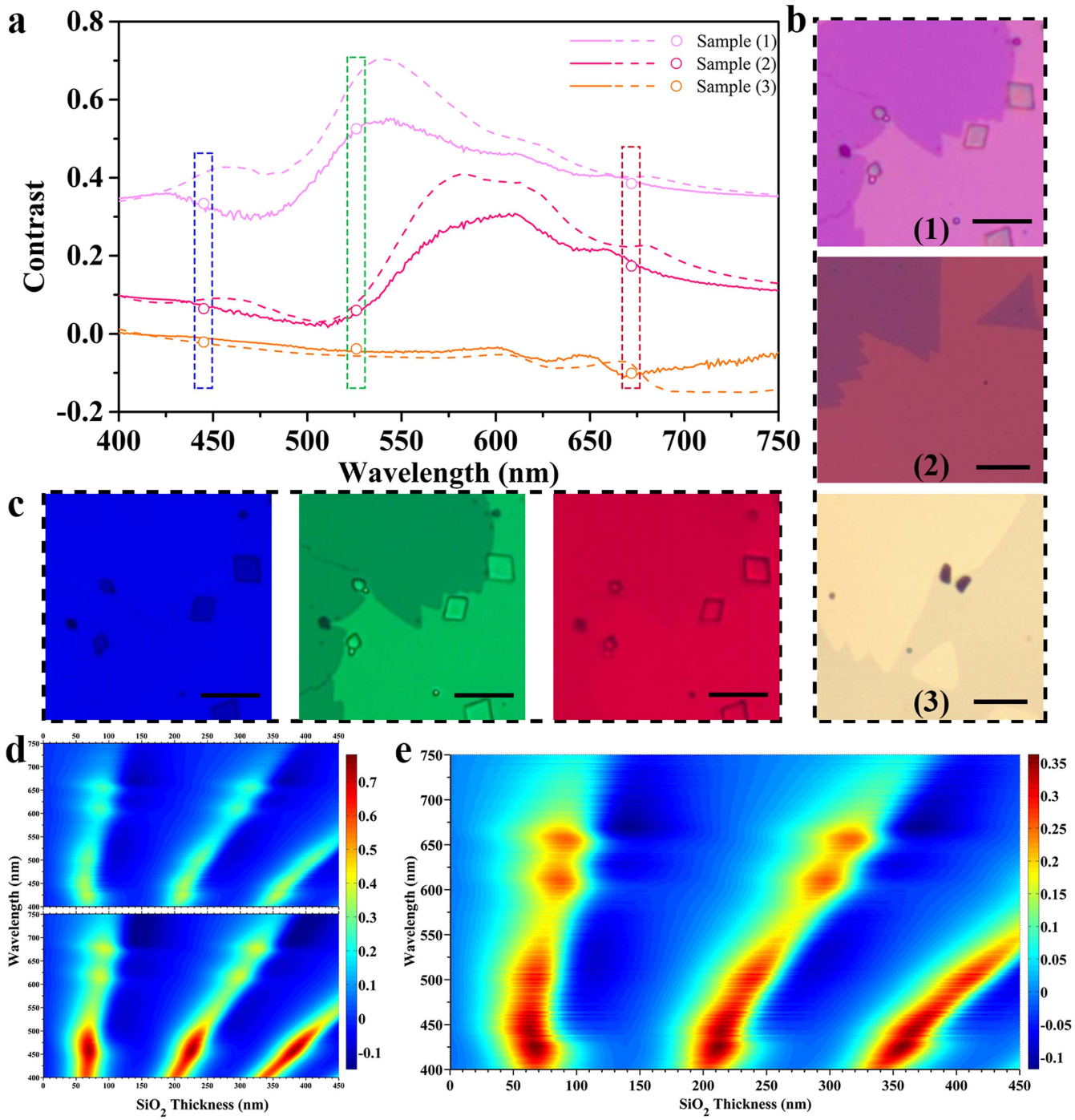

Figure 4 | Comparison of the optical contrasts of monolayer MoS_2 on SiO_2/Si substrates calculated with the refractive index of monolayer MoS_2 and that of bulk MoS_2. (a) Three representative contrast spectra of monolayer MoS_2 on different substrates, calculated with the refractive index of monolayer MoS_2 (solid lines), together with those calculated with the refractive index of bulk MoS_2 (dashed lines). The samples (1)–(3) correspond to SiO_2 thicknesses of 262, 281, and 150 nm, respectively. The scattered open circles are the contrast data obtained directly from the monochromatic images of the three samples. (b) The optical images of samples (1)–(3). (c) The monochromic (blue, green, and red) images of sample (1) under 445 nm, 526 nm, and 672 nm light illumination, respectively. (d) The upper and lower ones are the color contour plots of the contrast as a function of both SiO_2 thickness and incident light wavelength calculated using the refractive index of monolayer MoS_2 and that of bulk MoS_2, respectively. (e) The redrawing of the upper one in (d) using a different color bar. All the scale bars in Fig. 4 correspond to 10 μm.

reason why the peak located around 480 nm of the real part of refractive index spectrum for the bulk MoS_2 splits into two peaks for monolayer case is still unknown, and needs further study.

In order to demonstrate the difference of the refractive indices for monolayer and bulk MoS_2 from another point of view, we calculated three representative contrast spectra of monolayer MoS_2 on SiO_2/Si substrates, with SiO_2 thicknesses of 262, 281, and 150 nm, respectively, labeled as samples (1)–(3). The results are plotted (solid lines) together with those calculated using the refractive index of bulk MoS_2 (dashed lines) in Fig. 4a. Figure 4b shows the optical images of samples (1)–(3), respectively. The optical images show different colors as a result of the different reflectance spectra of the three samples.

We also took the monochromatic images of the samples by inserting narrow-band filters into the illuminating optical path. As an example, three monochromatic images of sample (1) are shown in Fig. 4c. The images show quite different contrast, the blue one having the worst contrast, and the green one having the best. From the converted grayscale images, we obtained the contrast data directly. The obtained contrast data for all the three samples are plotted in Fig. 4a (scattered open circles). We can see that the measured contrast data agree well with those calculated with the refractive index of monolayer MoS_2 (solid lines).

Using refractive indices of monolayer and bulk MoS_2, we calculated the color contour plots of the contrast as a function of both SiO_2 thickness and incident light wavelength for monolayer MoS_2 on SiO_2/Si substrate. The results were plotted in Fig. 4d under the same color bar. The clear difference between these two plots confirms again that the difference between the refractive indices of monolayer and bulk MoS_2 cannot be ignored. For both fundamental study and device application, it is useful to make the sample visible under an optical microscope. It is common to use 280 nm–300 nm SiO_2/Si substrates for monolayer MoS_2 in order to visualize it. In principle, with this color contour plot, one can make the monolayer MoS_2 visible on any SiO_2/Si substrate by selecting the proper incident light wavelength, and vice versa. For convenient to use, we replotted the color contour plot in Fig. 4e using a more appropriate color bar.

Discussion

In this work, we have synthesized highly crystalline monolayer MoS_2 on 26 different SiO_2/Si substrates with SiO_2 thickness ranging from ~130 nm to ~370 nm, and have devised a method to measure the contrast spectra of monolayer MoS_2 on these substrates. Using these contrast spectra, we extracted the complex refractive index spectrum of monolayer MoS_2 in the wavelength range of 400 nm to 750 nm. We have analyzed the pronounced difference between the obtained complex refractive index spectrum and that of bulk MoS_2. Furthermore, we have calculated the color contour plots of the contrast as a function of both SiO_2 thickness and incident light wavelength for monolayer MoS_2 using the obtained refractive index spectrum. These plots are useful for both fundamental study and device application. The measurement method presented here, with the advantage over conventional methods for 2D materials with small size, can be applied to other 2D materials which can be synthesized with good repeatability.

Methods

Preparation of SiO_2/Si substrates. We chemically etched the thermally oxidized SiO_2 capping layers on the Si substrates to various thicknesses (from 130 nm to 370 nm) using buffered hydrogen fluoride (HF) (HF (40%): NH_4F (8 M) = 1:10). The original thickness of the SiO_2 capping layer was 600 nm. The whole etching process was carried out in ice-bath with magnetic stirring. The thickness of the SiO_2 layer was measured by a thin film thickness measurement system (SpectraThick Series, ST2000-DLXn) with repeatability of 0.5 nm. The refractive index of the *p*-Si substrate (resistivity: 8–12 Ω·cm) was measured by an ellipsometer (Horiba Jobin Yvon Uvisel) (shown in Fig. S2).

Synthesis of monolayer MoS_2. We synthesized monolayer MoS_2 on SiO_2/Si substrates with a double-temperature-zone CVD method at ambient pressure. The MoO_3 (99.99%) and S (99.999%) powders, serving as the source, were loaded onto two quartz boats, respectively, which were later inserted into a 1-inch diameter quartz tube placed in a tubular furnace. The MoO_3 located at the downstream of high-purity argon (Ar) carrier gas. SiO_2/Si substrates were placed with faces down above MoO_3. During the synthesis process, the temperatures at MoO_3 and S sources were first raised to 100°C and kept there for 1 h with Ar gas flow rate of 120 sccm to exhaust water and air. Then the temperatures at MoO_3 and S were ramped to 650°C and 220°C, respectively, in 40 min, and kept there for 10 min, with Ar gas flow rate of 10 sccm. After that, the furnace was cooled down to room temperature without feedback with Ar gas flow rate of 10 sccm.

Characterization of monolayer MoS_2. The thickness and crystal structure of monolayer MoS_2 were characterized by AFM (Bruker Dimension Icon-PT) and TEM (Tecnai F30), respectively. For TEM sample preparation, we first spun a layer of poly (methyl methacrylate) (PMMA) onto a MoS_2/SiO_2/Si sample. Then we etched off the SiO_2 layer by KOH aqueous solution (2 M) and cleaned the floating PMMA/MoS_2 membrane several times with deionized water. Finally the membrane was scooped onto a TEM grid and dried. The PMMA was removed by annealing the TEM sample at 400°C for 3 h in an Ar/H_2 ambient. The PL and Raman spectra of monolayer MoS_2 were measured by a confocal Raman microscopic system (Horiba Labram HR800) at room temperature. The excitation laser wavelength was 488 nm.

Spatially resolved spectrum system. The spatially resolved reflectance spectrum was measured by using an optical microscopic spectrum system, which included an optical microscope (Zeiss Axio Imager. A2m) equipped with a halogen lamp (Zeiss Hal 100, 12 V, and 100 W), and a spectrometer (Horiba Jobin Yvon Triax 320). One end of an optical fiber was placed at the image plane of the microscope to selectively couple part of the light signal there to the spectrometer. The diameter of the optical fiber is 9 μm.

Obtaining Monochromatic Images. Monochromatic image was obtained by inserting a color filter with bandwidth of ~10 nm into the illuminating optical path of the optical microscope. The central wavelengths of the three filters used in Fig. 4 are 445 nm, 526 nm, and 672 nm, respectively.

1. Novoselov, K. S. *et al.* Electric field effect in atomically thin carbon films. *Science* **306**, 666–669 (2004).
2. Mak, K. F., Lee, C., Hone, J., Shan, J. & Heinz, T. F. Atomically thin MoS_2: A new direct-gap semiconductor. *Phys. Rev. Lett.* **105**, 136805 (2010).
3. Wang, Q. H., Kalantar-Zadeh, K., Kis, A., Coleman, J. N. & Strano, M. S. Electronics and optoelectronics of two-dimensional transition metal dichalcogenides. *Nat. Nanotechnol.* **7**, 699–712 (2012).
4. Ezawa, M. Spin-valley optical selection rule and strong circular dichroism in silicene. *Phys. Rev. B* **86**, 161407 (2012).
5. Xiao, D., Liu, G. B., Feng, W. X., Xu, X. D. & Yao, W. Coupled spin and valley physics in monolayers of MoS_2 and other group-vi dichalcogenides. *Phys. Rev. Lett.* **108**, 196802 (2012).
6. Zhu, Z. Y., Cheng, Y. C. & Schwingenschlogl, U. Giant spin-orbit-induced spin splitting in two-dimensional transition-metal dichalcogenide semiconductors. *Phys. Rev. B* **84**, 153402 (2011).
7. Cao, T. *et al.* Valley-selective circular dichroism of monolayer molybdenum disulphide. *Nat. Commun.* **3**, 887 (2012).
8. Mak, K. F., He, K. L., Shan, J. & Heinz, T. F. Control of valley polarization in monolayer MoS_2 by optical helicity. *Nat. Nanotechnol.* **7**, 494–498 (2012).
9. Zeng, H. L., Dai, J. F., Yao, W., Xiao, D. & Cui, X. D. Valley polarization in MoS_2 monolayers by optical pumping. *Nat. Nanotechnol.* **7**, 490–493 (2012).
10. Sallen, G. *et al.* Robust optical emission polarization in mos2 monolayers through selective valley excitation. *Phys. Rev. B* **86**, 081301 (2012).
11. Shan, W. Y., Lu, H. Z. & Xiao, D. Spin hall effect in spin-valley coupled monolayers of transition metal dichalcogenides. *Phys. Rev. B* **88**, 125301 (2013).
12. Li, Z. & Carbotte, J. P. Longitudinal and spin-valley hall optical conductivity in single layer MoS_2. *Phys. Rev. B* **86**, 205425 (2012).
13. Yin, X. B. *et al.* Edge nonlinear optics on a MoS_2 atomic monolayer. *Science* **344**, 488–490 (2014).
14. Hong, X. P. *et al.* Ultrafast charge transfer in atomically thin mos2/ws2 heterostructures. *Nat. Nanotechnol.* **9**, 682–686 (2014).
15. Lee, C. H. *et al.* Atomically thin p-n junctions with van der waals heterointerfaces. *Nat. Nanotechnol.* **9**, 676–681 (2014).
16. Furchi, M. M., Pospischil, A., Libisch, F., Burgdorfer, J. & Mueller, T. Photovoltaic effect in an electrically tunable van der waals heterojunction. *Nano Lett.* **14**, 4785–4791 (2014).
17. Cheng, R. *et al.* Electroluminescence and photocurrent generation from atomically sharp wse2/mos2 heterojunction p-n diodes. *Nano Lett.* **14**, 5590–5597 (2014).
18. Lee, Y. H. *et al.* Synthesis of large-area MoS_2 atomic layers with chemical vapor deposition. *Adv. Mater.* **24**, 2320–2325 (2012).
19. Najmaei, S. *et al.* Vapour phase growth and grain boundary structure of molybdenum disulphide atomic layers. *Nat. Mater.* **12**, 754–759 (2013).
20. Van Der Zande, A. M. *et al.* Grains and grain boundaries in highly crystalline monolayer molybdenum disulphide. *Nat. Mater.* **12**, 554–561 (2013).
21. Beal, A. R. & Hughes, H. P. Kramers-Kronig analysis of the reflectivity spectra of 2h- MoS_2, 2h-$MoSe_2$ and 2h-$MoTe_2$. *J. Phys. C: Solid State Phys.* **12**, 881–890 (1979).
22. Yim, C. Y. *et al.* Investigation of the optical properties of mos2 thin films using spectroscopic ellipsometry. *Appl. Phys. Lett.* **104**, 103114 (2014).
23. Eichfeld, S. M., Eichfeld, C. M., Lin, Y. C., Hossain, L. & Robinson, J. A. Rapid, non-destructive evaluation of ultrathin wse2 using spectroscopic ellipsometry. *APL Mat.* **2**, 092508 (2014).
24. Liu, H. L. *et al.* Optical properties of monolayer transition metal dichalcogenides probed by spectroscopic ellipsometry. *Appl. Phys. Lett.* **105**, 201905 (2014).
25. Blake, P. *et al.* Making graphene visible. *Appl. Phys. Lett.* **91**, 063124 (2007).
26. Benameur, M. M. *et al.* Visibility of dichalcogenide nanolayers. *Nanotechnology* **22**, 125706 (2011).
27. Splendiani, A. *et al.* Emerging photoluminescence in monolayer MoS_2. *Nano Lett.* **10**, 1271–1275 (2010).

28. Eda, G. *et al.* Photoluminescence from chemically exfoliated MoS_2. *Nano Lett.* **11**, 5111–5116 (2011).
29. Li, S. L. *et al.* Quantitative raman spectrum and reliable thickness identification for atomic layers on insulating substrates. *ACS Nano* **6**, 7381–7388 (2012).
30. Mak, K. F. *et al.* Measurement of the optical conductivity of graphene. *Phys. Rev. Lett.* **101**, 196405 (2008).
31. Rydberg, H. *et al.* Van der waals density functional for layered structures. *Phys. Rev. Lett.* **91**, 126402 (2003).
32. Zhao, W. J. *et al.* Evolution of electronic structure in atomically thin sheets of WS_2 and WSe_2. *ACS Nano* **7**, 791–797 (2013).
33. Evans, B. & Young, P. Optical absorption and dispersion in molybdenum disulphide. *Proc. R. Soc. Lond. A* **284**, 402–422 (1965).

Acknowledgments

The authors would like to thank Dr. W.L. Chen for improving the English writing of this paper. This work was supported by the National Basic Research Program of China (Nos. 2013CB921901 and 2012CB932703), and the National Natural Science Foundation of China (Nos. 61125402, 51172004, and 11474007).

Author contributions

L.D. and H.Z. conceived the research, analyzed the data, and wrote the manuscript. Y.M. and H.Z. devised the optical contrast spectra measurement method. H.Z. and Y.W. synthesized the samples, did the PL, Raman, and optical contrast spectra measurements. X.R. did the AFM measurement. Z.X. measured the refractive index of silicon. H.Z. did the TEM characterization and the numerical calculation (assisted by W.W.). L.D. supervised the study. All authors discussed the results.

Additional information

Supplementary information accompanies this paper at http://www.nature.com/scientificreports

Competing financial interests: The authors declare no competing financial interests.

How to cite this article: Zhang, H. *et al.* Measuring the Refractive Index of Highly Crystalline Monolayer MoS_2 with High Confidence. *Sci. Rep.* **5**, 8440; DOI:10.1038/srep08440 (2015).